Estimation of 3D deformation and rotation rate tensor from volumetric particle data via 3D least squares matching

J. Kitzhofer[1], P. Westfeld[2], O. Pust[3], T. Nonn[3], H. G. Maas[2] and C. Brücker[1]

1: Institute of Mechanics and Fluid Dynamics, University of Freiberg, Germany, jens.kitzhofer@imfd.tu-freiberg.de
2: Institute of Photogrammetrie, University of Dresden, Germany
3: Dantec Dynamics A/S, Skovlunde, Denmark

Abstract This article discusses the estimation of the deformation rate and rotation rate tensor from results obtained by 3D Least Squares Matching (LSM), which is applied to volumetric voxel spaces for the calculation of 3D velocity fields. It is shown that LSM already yields the velocity gradient matrix for computation of the deformation and rotation rate tensor. Vorticity, shear and strain are calculated without applying central differences schemes. It is shown that LSM is well suited for the extraction of the deformation parameters in cases of small to medium deformations. The accuracy and constraints will be pointed out by analyzing the coefficients of the tensors. Results are presented for simulated and experimental datasets.

1. Introduction

In the last decades several investigations have been performed to experimentally describe the motion of fluid. The fundamental theorem by Helmholtz says that every infinitesimal motion of a fluid element can be decomposed in translation, rotation and deformation.
Initially, the measurement technique Particle Image Velocimetry (PIV) was used for 2D investigations yielding a planar field with translational velocities in the Eulerian frame [1]. Thus, only one part of the fundamental theorem could be described in 2D. Developments like Scanning PIV [2], Holographic PIV [3] and Tomographic PIV [4] expanded the description of fluid motion to 3D. Here, correlation based techniques, like 3D cross correlation, are frequently applied in the post processing on gray value voxel spaces to extract the zero order translational velocity components neglecting the higher order terms of rotation and deformation. The assumption is that the flow field is smooth and not significantly influenced by rotational or shear displacements, thus yielding the zero-order translational displacement field with an additional uncertainty in measurement due to neglecting the higher-order terms. Reduction of the measurement uncertainty can be achieved by window deformation techniques [5]. The higher-order motion terms are then estimated by finite difference schemes of the velocity field information on discrete grids (indirectly by consideration of the translational velocities of neighbouring elements). The assumption is that the higher order fluid motion of an element is only affected by the translational velocity components of the neighbouring elements.
Another approach for estimation of velocity fields is Least Squares Matching (LSM) [6]. LSM has already been successfully used in the analysis of 2D particle images. Nevertheless, cross correlation techniques outperformed LSM because of the shorter processing times. In contrast to correlation based techniques, Least Squares Matching (LSM) shifts, rotates and stretches a fluid area. For this purpose, the least squares matching algorithm iteratively compares gray value information of an interrogation area in the first time step with the gray value information in the second time step. This is an iterative least squares procedure applying an affine transformation on the interrogation areas. In 2D this results in six transformation parameters and in 3D this results in twelve transformation parameters for each interrogation area.
So, the advantage of LSM is that while calculating the zero order translational velocities, the first

order terms of motion are considered increasing the accuracy of the velocity field. Moreover, the affine transformation includes parameters like rotation, shear and strain of the interrogation area. This paper shows how to extract these parameters from the affine transformation and to transform them in the description of fluid motion.
For this purpose, this article first discusses the necessary principles (fundamental theorem of fluid motion, Least Squares Matching) and the connection of both principals to calculate the deformation rate and rotation rate tensor via the results obtained by LSM. A parametric study is performed on a single volumetric cube to show the accuracy and the constraints of the estimation of deformation and rotation rate. A simulated Hill type vortex shows the strength of the method for identifying regions in the flow of high fluid mechanical interest. At the end we will show results for the benchmark experiment of a vortex ring.

2. Principles

This section summarizes the basic principles for understanding the estimation of the rotation and deformation rate tensor via the dataset obtained by 3D Least squares matching. For this purpose, the fundamental theorem for fluid motion is shortly described. The equivalent description in terms of transforming one system (basic cube) into another system (deformed cube) as obtained by 3D LSM is discussed and both mathematical descriptions are compared showing that 3D LSM yields the velocity gradient matrix and consequently the rotation and deformation rate tensor.

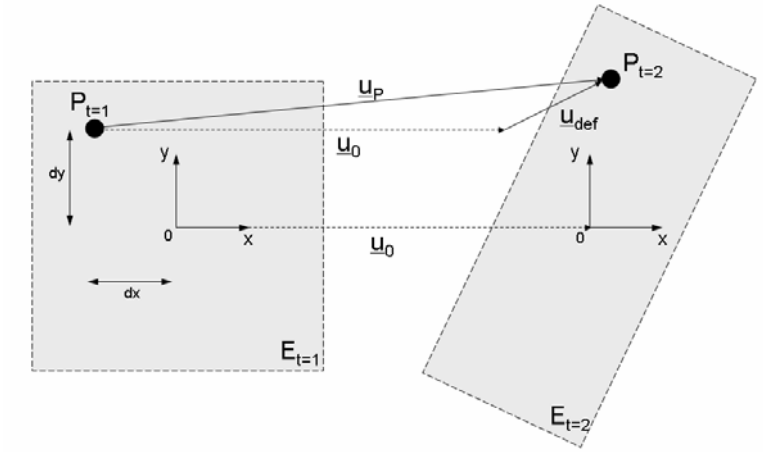

Fig 1. Definition of fluid motion: E represents the fluid element at two successive time steps; P is a point inside the infinitesimal fluid element; the velocity of P ($\underline{u}_P$) is the sum of the translational velocity $\underline{u}_0$ and the deformation velocity $\underline{u}_{def}$

2.1 Fundamental theorem of fluid motion

The fundamental theorem by Helmholtz says that the velocity at a point $\underline{x}+d\underline{x}$ inside an infinitesimal fluid element E at $\underline{x}$ can be decomposed in a constant translational velocity $\underline{u}_0(\underline{x})$ of the fluid element and in a velocity $\underline{u}_{def}(d\underline{x})$ resulting from the deformation of the fluid element as a function of the distance $d\underline{x}$ from the center of the fluid element as shown in figure 1. Mathematically, this is written:

$$\underline{u}(\underline{x}+d\underline{x},t) = \underline{u}_0(\underline{x},t) + \underline{u}_{def}(d\underline{x}) \quad (1)$$

The velocity at $d\underline{x}$ in the infinitesimal volume element resulting from deformation is written in

terms of the velocity gradient matrix $\underline{\underline{V}}$:

$$\underline{u}_{def}(d\underline{x}) = \begin{bmatrix} \frac{\partial u}{\partial x} & \frac{\partial u}{\partial y} & \frac{\partial u}{\partial z} \\ \frac{\partial v}{\partial x} & \frac{\partial v}{\partial y} & \frac{\partial v}{\partial z} \\ \frac{\partial w}{\partial x} & \frac{\partial w}{\partial y} & \frac{\partial w}{\partial z} \end{bmatrix} d\underline{x} = \underline{\underline{V}} \cdot d\underline{x} \quad (2)$$

It is generally that the Jacobian of the velocity can be decomposed in a symmetric tensor $\underline{\underline{D}}$ and an asymmetric tensor $\underline{\underline{R}}$, where $\underline{\underline{R}}$ describes the rotation rate tensor and $\underline{\underline{D}}$ the deformation rate tensor.

$$\underline{\underline{V}} = \underline{\underline{R}} + \underline{\underline{D}} \quad (3)$$

The deformation rate tensor describes strain $\varepsilon_{ij,\ i=j}$ and shear $\varepsilon_{ij,\ i\neq j}$ of the infinitesimal volume element resulting from velocity gradients in the inner of the volume.

$$\underline{\underline{D}} = \begin{pmatrix} \frac{\partial u}{\partial x} & \frac{1}{2}\left(\frac{\partial v}{\partial x} + \frac{\partial u}{\partial y}\right) & \frac{1}{2}\left(\frac{\partial u}{\partial z} + \frac{\partial w}{\partial x}\right) \\ \frac{1}{2}\left(\frac{\partial v}{\partial x} + \frac{\partial u}{\partial y}\right) & \frac{\partial v}{\partial y} & \frac{1}{2}\left(\frac{\partial w}{\partial y} + \frac{\partial v}{\partial z}\right) \\ \frac{1}{2}\left(\frac{\partial u}{\partial z} + \frac{\partial w}{\partial x}\right) & \frac{1}{2}\left(\frac{\partial w}{\partial y} + \frac{\partial v}{\partial z}\right) & \frac{\partial w}{\partial z} \end{pmatrix} = \begin{bmatrix} \varepsilon_{xx} & \varepsilon_{xy} & \varepsilon_{xz} \\ \varepsilon_{yx} & \varepsilon_{yy} & \varepsilon_{yz} \\ \varepsilon_{zx} & \varepsilon_{zy} & \varepsilon_{zz} \end{bmatrix} \quad (4)$$

The rotation rate tensor describes the vorticity ω in each spatial direction x, y, z.

$$\underline{\underline{R}} = \begin{bmatrix} 0 & -\frac{1}{2}\left(\frac{\partial v}{\partial x} - \frac{\partial u}{\partial y}\right) & \frac{1}{2}\left(\frac{\partial u}{\partial z} - \frac{\partial w}{\partial x}\right) \\ \frac{1}{2}\left(\frac{\partial v}{\partial x} - \frac{\partial u}{\partial y}\right) & 0 & -\frac{1}{2}\left(\frac{\partial w}{\partial y} - \frac{\partial v}{\partial z}\right) \\ -\frac{1}{2}\left(\frac{\partial u}{\partial z} - \frac{\partial w}{\partial x}\right) & \frac{1}{2}\left(\frac{\partial w}{\partial y} - \frac{\partial v}{\partial z}\right) & 0 \end{bmatrix} = \begin{pmatrix} 0 & -\omega_z & \omega_y \\ \omega_z & 0 & -\omega_x \\ -\omega_y & \omega_x & 0 \end{pmatrix} \quad (5)$$

It is obvious that calculation of the deformation rate and rotation rate tensor for fully describing fluid motion needs the evaluation of the velocity gradient matrix $\underline{\underline{V}}$.

2.2 3D Least Squares Matching (3D LSM)

The basic principle of Least Squares Matching is the evaluation of a transformation, which transforms the state of a system into another state of the same system. For this purpose the states of the system are compared via an iterative least squares procedure. In the application of 3D LSM to volumetric particle data as obtained by Tomo PIV, the system is an interrogation volume (cuboid) and the state of the system is the gray value representation of particles. The transformation is evaluated in an iterative least square adjustment procedure, where the gray values in state one are transformed into the gray values in state two. A detailed description can be seen in [7]. The geometrical model is an affine transformation for each cuboid E transforming all positions at state

one in the inner of the cuboid into the positions at state 2.

$$\left.\begin{aligned} x_2 &= a_0 + a_1 \cdot dx_1 + a_2 \cdot dy_1 + a_3 \cdot dz_1 \\ y_2 &= b_0 + b_1 \cdot dx_1 + b_2 \cdot dy_1 + b_3 \cdot dz_1 \\ z_2 &= c_0 + c_1 \cdot dx_1 + c_2 \cdot dy_1 + c_3 \cdot dz_1 \end{aligned}\right|_E \quad (6)$$

The index 1 means the state of the volume element at time step 1 and the index 2 the state of the volume element at time step 2. The parameters a_0, b_0 and c_0 are the constant translational displacements valid for each point in the infinitesimal cuboid E. In the following the translational displacements in the cuboid E at $\underline{x}$ will be $\underline{t}_0(\underline{x}) = (a_0, b_0, c_0)^T$ directly yielding the translational velocity of all points in the cuboid E at $\underline{x}$.

$$\underline{u}_0(x) = \frac{\underline{t}_0}{\Delta t} \quad (7)$$

The deformation of the cuboid is described by the transformation matrix $\underline{\underline{T}}$:

$$\underline{\underline{T}} = \begin{bmatrix} a_1 & a_2 & a_3 \\ b_1 & b_2 & b_3 \\ c_1 & c_2 & c_3 \end{bmatrix}_E = \begin{bmatrix} \frac{\partial x_2}{\partial x_1} & \frac{\partial x_2}{\partial y_1} & \frac{\partial x_2}{\partial z_1} \\ \frac{\partial y_2}{\partial x_1} & \frac{\partial y_2}{\partial y_1} & \frac{\partial y_2}{\partial z_1} \\ \frac{\partial z_2}{\partial x_1} & \frac{\partial z_2}{\partial y_1} & \frac{\partial z_2}{\partial z_1} \end{bmatrix}_E \quad (8)$$

2.3 Velocity gradient matrix

The velocity gradient matrix is necessary for the computation of the deformation and rotation rate tensor. The result from LSM is the transformation matrix und the displacement vector. So, for a given point $P_1 = (dx, dy, dz)^T$ in the inner of the cuboid E the position of the point P_2 is calculated via the transformation matrix assuming that the translational displacement is zero:

$$P_2 = \underline{\underline{T}} \cdot P_1 \quad (9)$$

The velocity of the point due to the deformation is calculated by:

$$\underline{u}_{def}(d\underline{x}) = \frac{P_2 - P_1}{\Delta t} = \frac{\underline{\underline{T}} \cdot P_1 - P_1}{\Delta t} = \frac{(\underline{\underline{T}} - \underline{\underline{I}})}{\Delta t} \cdot P_1, \underline{\underline{I}} = \begin{bmatrix} 1 & 0 & 0 \\ 0 & 1 & 0 \\ 0 & 0 & 1 \end{bmatrix} \quad (10)$$

So, by comparison of (2) and (10) it is clear that the velocity gradient matrix $\underline{\underline{V}}$ of a volume element E and as a consequence the rotation rate $\underline{\underline{R}}$ and deformation rate tensor $\underline{\underline{D}}$ is derived by subtracting the identity tensor $\underline{\underline{I}}$ from the transformation matrix $\underline{\underline{T}}$ and by following division by the separation time Δt.

$$\underline{\underline{V}} = \frac{(\underline{\underline{T}} - \underline{\underline{I}})}{\Delta t} \quad (11)$$

3. Numerical assessment

In this section we present numerical results for the estimation of the rotation rate and deformation rate tensor obtained by LSM. The accuracy of the estimation is analysed via synthetic generated voxel spaces. For this purpose a parametrical study is performed by analysing the deformation of a well defined cube. The interpretation of fluid mechanical aspects is shown at the end via a simulated Hill type vortex.

3.1 Cube deformation

The following parametrical study extracts influences on the estimation of the rotation rate and deformation rate tensor. Parameters are number of particles, noise and strength and number of deformation. The synthetic set-up is shown in figure 2. A cubic element (60x60x60 voxel) is generated with the coordinate system in the center of gravity. A part of the element (40x40x40) is then filled with homogenous sized particles (3x3x3 voxel elements) at random positions having a Gaussian intensity distribution. The positions of the particles are chosen with sub pixel accuracy and represent the original cube without deformations. The particle positions are then deformed via defined shearings and strains and following rotations. The shifted particle positions represent the deformed cube. The undeformed and deformed cubes are then analysed via LSM to calculate the transformation matrix and in the following processing step the velocity gradient matrix. The computation of the LSM parameter is performed by an adapted code given by Thomas Nonn from Dantec Dynamics.

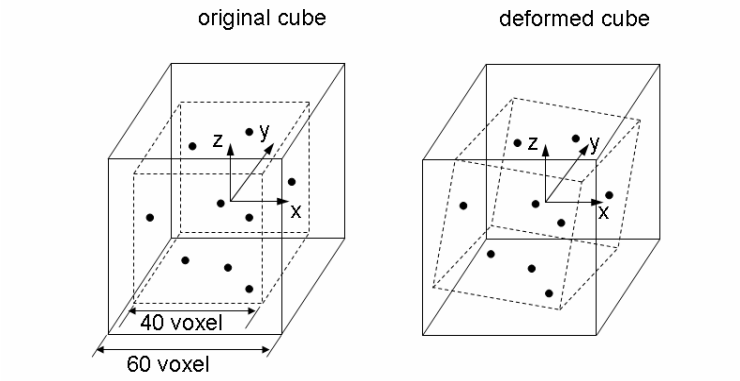

Fig 2. Numerical set-up for the parametrical study of the cube deformation

As LSM is an iterative least squares procedure, it is sensitive to starting values. The analysis herein is performed without the knowledge of starting values resulting in a higher number of necessary iteration steps to calculate the transformation matrix within predefined boundaries. To make the result independent of the number of iteration steps, the iterative procedure is stopped after 200 iterations, which is far beyond necessarily about 10 iterations for small deformations [10].
In the following the value dev is defined as the relative accuracy of the measured deformations, where σ_{calc} is the calculated value (ω_i, ε_{ij}) and σ_0 is the initial value (ω_{i0}, ε_{ij0}):

$$dev = \frac{\left|\sigma_{calc} - \sigma_0\right|}{\sigma_0} \cdot 100\%$$

Figure 3 on the left shows the accuracy of the absolute value of rotation as a function of particle per pixel (ppp). Particle per pixel is defined by generated number of particle positions divided by the

size of one side of the cube (herein 40x40 pix²). The deformation consists of rotations around each axis and strain and shear in two planes representing a cube with low magnitude in deformation but large number of different deformations. At low particle densities the error is very high up to 80 % converging to 10 % within a slightly increasing ppp. Common 2D PIV images have a number particle density of 0.1... 0.2 ppp. This is much higher than the observed border at 0.005 ppp in figure 1. This is in agreement with [8]. They used a 2D LSM approach for Particle Tracking Velocimetry, which measures velocities at lower number particle density. Nevertheless, the following investigations will be performed at 0.1 ppp, because the aim of this paper is the application of LSM to Tomo PIV. But to point out, LSM delivers a constant accuracy of 10 % beyond 0.005 ppp.

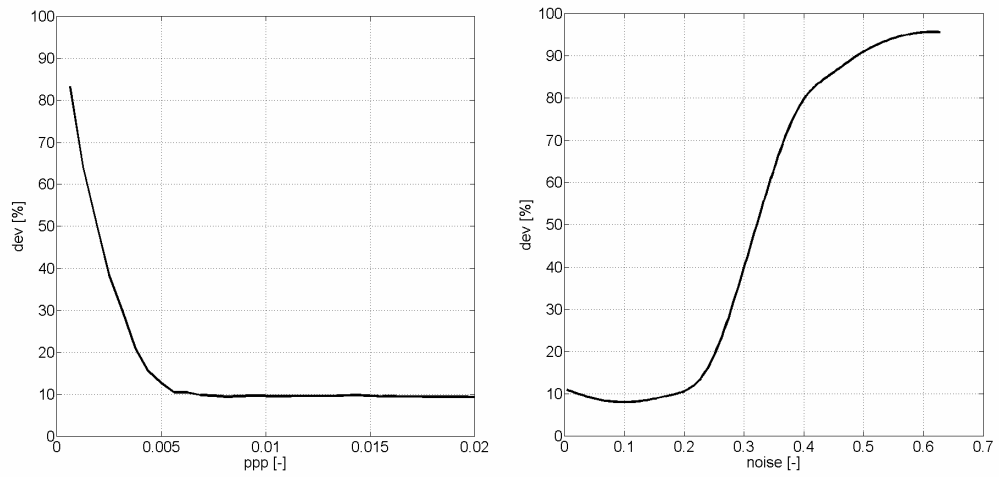

Fig 3. Accuracy in measurement;
left: as a function of ppp (deformation: $\omega = \varphi = \kappa = 5°$; $d_{xx} = 1.1$, $d_{yy} = 0.9$, $d_{zz} = 1$; $d_{xy} = 0.1$, $d_{xz} = 0.1$, $e_{yz} = 0$);
right: as function of noise (deformation: $\omega = 12$; $\varphi = \kappa = 10°$; $d_{xx} = 1$, $d_{yy} = 1$, $d_{zz} = 1$; $d_{xy} = 0$, $d_{xz} = 0$, $e_{yz} = 0$)

Figure 3 on the right shows the deviation as a function of noise. Noise is included in a way that the gray value of each voxel position is superimposed by a randomly standard deviation. The maximum standard deviation is defined between 0 and 255 meaning noise 0 is a standard deviation of 0 and noise 1 is a standard deviation of 255. It is clearly recognizable that dev increases to more than 10 % from a noise of 0.2. This that LSM is applicable, if the noise does not increase 20 % of the highest magnitude in the images, herein 255. The reason probably is that the shapes of the particles start to smear with the surrounding.
The relative deviation in absolute rotational strength as a function of increasing rotational strength (increasing deformation) shows figure 4. The solid line shows the deviation for ω_y ,$\omega_z = 0°$ and the dashed line shows the deviation for ω_y ,$\omega_z = 15°$. The solid line remains nearly constant up to a rotation in x-direction of about 15°. The deviation is pretty low (< 3%). Between 15° and 20° the deviation dramatically increases being beyond 10% at about 22°. If rotations around the other axes are included, two characteristics can be concluded (dashed line). The deviation for small rotations is increased (≈ 7%) and the sudden increase of the deviation is shifted to lower values of ω_x. This problem is well known in literature and results from the assumption of the affine transformation. The transformation is linear, which is valid for small deformations. But when the absolute deformation is increased, the transformation becomes non-linear.

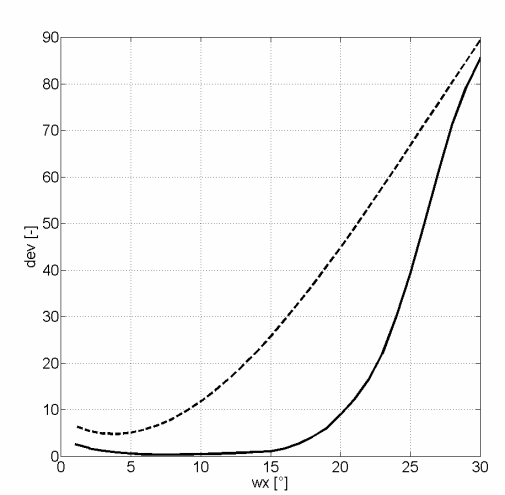

Fig 4. Accuracy in measurement as a function of ω_x
(deformations: $\varphi = \kappa = 0°$ -solid- /15° -dashed-; $d_{xx} = 1$ $d_{yy} = 1$, $d_{zz} = 1$; $d_{xy} = 0$, $d_{xz} = 0$, $d_{yz} = 0$)

Figure 5 shows the influences on the accuracy on shear and strain. In both classes of deformation trends are visible. On the one hand the deviation again dramatically increases, when a certain deformation is exceeded. On the other hand the deviation increases for lower deformation, if multiple deformations are included. Nevertheless, the deviation of strain and shear is in the order of magnitude of about 1% remaining nearly constant also in the case if multiple deformations are included.

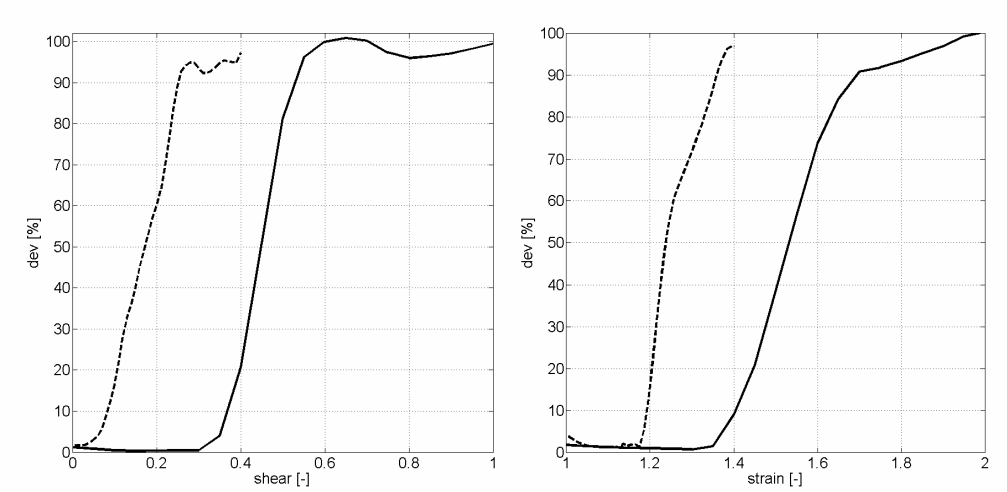

Fig 5. Accuracy in measurement;
left: as a function of shear in xy (deformations: $\omega = \varphi = \kappa = 0°$; $d_{xx} = 1$ $d_{yy} = 1$, $d_{zz} = 1$; $d_{xz} = 0$ -solid- /0.3 -dashed-, $d_{yz} = 0$ -solid- /0.3 -dashed-);
right: as a function of strain in x (deformations: $\omega = \varphi = \kappa = 0°$; $d_{xx} = 1$ $d_{yy} = 1$, $d_{zz} = 1$; $d_{xz} = 0$ -solid- /0.3 -dashed-, $d_{yz} = 0$ -solid- /0.3 -dashed-)

The parametrical study of the cube deformation shows that LSM can handle multiple deformations up to certain strength. The accuracy is in the order of 1% if only one class of deformation is included. If multiple classes of deformation are included, the accuracy decreases to about 10 %. Nevertheless, strong deformations are not capable of the LSM algorithm. The reason is probably in the assumption of an affine transformation.

3.2 Hill type vortex

In the numerical assessment we use the hill type vortex ring for validation of the extraction of the deformation and rotation rate tensor from the LSM results. The hill type vortex is characterized by spherical streamlines, a donut like vortex core and two stagnation points (upstream and downstream). The exact solution of the Navier Stokes equations for the inner part (r<R) is written in cylindrical coordinates:

$$U_R = -1.5 \cdot U_0 \cdot \cos(\Phi) \cdot \left(1 - \frac{r^2}{R^2}\right)$$

$$U_\Phi = 1.5 \cdot U_0 \cdot \sin(\Phi) \cdot \left(1 - \frac{2r^2}{R^2}\right)$$

U_R is the radial velocity, U_Φ is the circumferential velocity and U_0 is the transport velocity of the vortex. For the outer part of the vortex (r>R) the solution is written:

$$U_R = U_0 \cdot \cos(\Phi) \cdot \left(1 - \frac{R^3}{r^3}\right)$$

$$U_\Phi = 1.5 \cdot U_0 \cdot \sin(\Phi) \cdot \left(1 - \frac{R^3}{2r^3}\right)$$

As the LSM algorithm is defined in Cartesian coordinates, the velocity field is transformed from cylindrical coordinates into Cartesian coordinates. The size of the generated velocity field is 101x101x101 voxel. The Cartesian grid is then filled with 1000 homogenous sized particles (3x3x3 voxel) with a Gaussian intensity distribution, meaning that 9% of the whole volume is filled with particles. The sub-pixel displacement of the particles due to the velocity field is then estimated with a Runge-Kutta scheme. Afterwards random noise with standard deviation of 1.5 is superimposed. The chosen conditions (random particle positions and noise) are a good approximation for real experimental conditions. The size of the analyzed cuboids is 15x15x15 voxel with an overlap of 75%. This results in 10648 translational displacements and transformation tensors.

The visualization of some results shows figure 6. The figure shows the velocity vectors in the symmetry plane x-z, the 3D streamlines starting above the upstream stagnation point, and isosurfaces of the vorticity magnitude (gray), the positive (orange) and the negative (blue) strain. Moreover, some numerical results of the deformation rate and rotation rate tensor are included. The generated streamlines clearly follow the exact solution of the hill type cortex. The streamlines form a spherical shape. The velocity vectors in the symmetry plane identify the velocity distribution of a hill type vortex. No outliers are recognizable. The isosurfaces of vorticity and strain excluded from the transformation matrix derived by LSM identify the main features of the hill type vortex without any further post processing steps. The upper and lower stagnation points are highlighted. The volume elements in the upper stagnation point are compressed in z-direction and expanded in x- and y-direction ($\varepsilon_{zz}<0$, $\varepsilon_{xx}>0$, $\varepsilon_{yy}>0$). In the lower stagnation point the scene is inverted. The isosurface of the vorticity magnitude identifies the donut like vortex core. The numerical result for the rotation rate tensor in the symmetry plane x-z at the vortex core for x<0 and x>0 is given. The prefixes of the entries for vorticity ω_y agree with the physical interpretation.

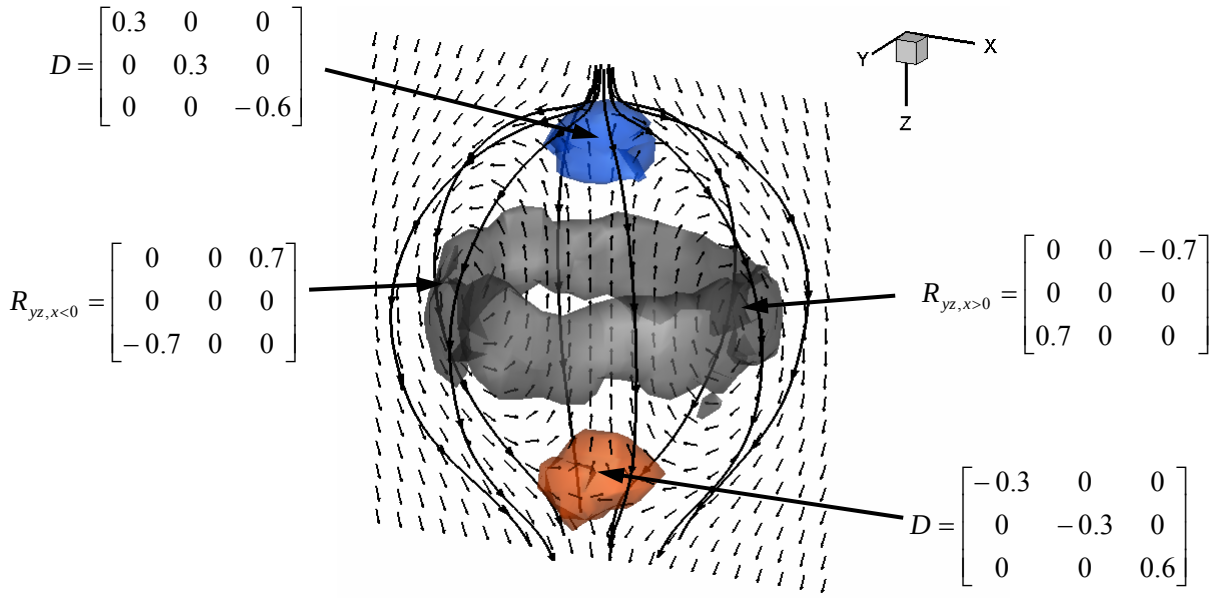

Fig 6. Visualization of some results obtained by LSM applied to the simulated hill type vortex ring; isosurface of vorticity magnitude (blue) identifies the donut like vortex core, isosurface of positive (red) and negative (blue) strain rates identify stagnation points; 3D streamlines show a spherical shape and the velocity vectors in the symmetry plane y-z characterize the velocity field of the hill type vortex

The numerical results show that the estimation of the rotation and deformation rate tensor via LSM delivers correct results without an exhausting post processing via central derivatives. The cube deformation showed an accuracy of about 1 % for small and single deformations and 10 % for small and multiple deformations. The Hill type vortex showed that physical aspects can simply be excluded from LSM.

4. Experiment

The experimental set-up is shown in figure 7. The laser beam of a continuous Argon-Ion laser Coherent Innova 70 (2 W) passes an optical lens system to adjust the desired thickness of the light sheet. The rotating mirror drum reflects the laser beam into the direction of the observed volume and generates successively 10 parallel light sheet planes with a thickness of 10 mm. The studied flow is a vortex ring travelling in an octagonal glass tank filled with water. The vortex is generated at the exit of a piston tube with a diameter of 50 mm. The neutrally buoyant seeding particles (100 microns) are injected into the center of the vortex generator. The particle images are recorded with a three camera system consisting of digital high speed cameras Photron APX RS with a resolution of 1024 x 1024 Pixel² and an angular displacement of 45°, -45° and 90°. The cameras are equipped with telecentric lenses at f-number 16 resulting in a parallel projection for the observed volume. The side of the octagon opposite to the entrance side for the laser is covered with a light absorbing mat that reduces stray reflections. This is also valid for the faces opposite the cameras, thus giving a perfectly black background. The experiments are performed with a recording rate of 1000 frames/s. Using 10 scanning planes results in a separation time of 10 ms for each subsequent illumination of one scan plane. The image size of the cameras and the light sheet thickness define the measured volume, resulting in about 90 x 90 x 10 mm³ for one light sheet.

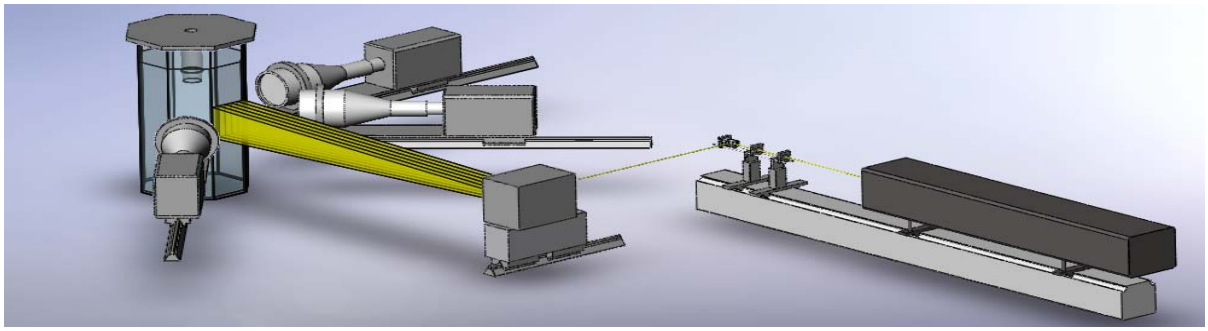

Fig 7 Experimental set-up consisting of three high speed cameras APX RS equipped with telecentric lenses

The volumetric reconstruction as well as LSM is performed by Dantec Dynamics Software. The volumetric reconstruction bases on a multiple projective transformation of each camera view into the depth layer of the observed volume and a minstore algebraic reconstruction technique. For further information on the volumetric reconstruction see [10]. In total a regular grid of 278x1112x944 voxel with gray value information is generated for each time step. The velocity field as well as the parameters of the affine transformation is calculated as presented in [7]. To summarize, the LSM algorithm is performed on 25^3 cuboids resulting in 25^3 velocity vectors and transformation matrices. The result is visualized in figure 8. The vortex ring is clearly recognizable. Beside the velocity vectors the isosurface of vorticity magnitude is included. To point out, the vorticity magnitude is not calculated via central difference schemes, but via the parameters of the affine transformation.

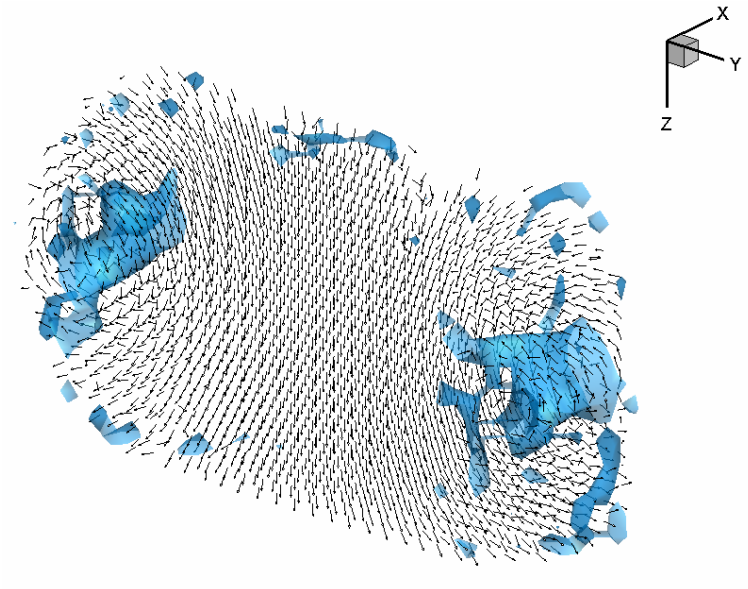

Fig 8 Vortex ring: the velocity vectors have a uniform length; the blue isosurface represents the vorticity magnitude showing the vortex core

5. Conclusion

The article discussed the estimation of the rotation and deformation rate tensor via the affine parameters resulting from LSM. It is shown that the calculation is straight forward without using any central difference schemes. The accuracy is estimated via the deformation of a well defined cube. The result is that LSM is valid for small multiple deformations and for medium single deformations. The accuracy is about 1% for single deformations and under 10 % for multiple

deformations. It seems that LSM is not sensible to high deformation rate, but sensible to high deformations. The extraction of the parameters is performed on a simulated as well as on an experimental vortex ring, both showing that the physical character of the vortex ring is described by the parameters of the affine transformation. Future work has to be performed in cases of large deformations. Here, the linear affine transformation needs to be replaced by a non linear model.

References

[1] Adrian RJ (1991) Particle-imaging techniques for experimental fluid mechanics. Ann Rev Fluid Mech 23:261-304
[2] Ch Brücker 1997 3D scanning PIV applied to an air flow in a motored engine using digital high-speed video. Meas. Sci. Technol. 8
[3] Soria J and Atkinson C (2008) Towards 3C-3D digital holographic fluid velocity vector field measurement-tomographic digital holographic PIV (Tomo-HPIV). Meas. Sci. Technol. 19
[4] Elsinga GE (2008) Tomographic Particle Image Velocimetry, Ph.D. Thesis, Department of Aerospace Engineering, Delft University of Technology
[5] Scarano F (2002) Iterative image deformation methods in PIV, Meas. Sci. Technol 13
[6] Tropea C, Yarin A, Foss JF (2007) Springer Handbook of Experimental Fluid Mechanics
[7] Westfeld P, Maas HG, Pust O, Kitzhofer J, Brücker C (2010) 3-D Least Squares Matching for Volumetric Velocimetry Data Processing, accepted for publication in the Proceedings of the 15th International Symposium on Appliocations of Laser Techniques to Fluid Mechnaics, 5-8 July 2010, Lisbon
[8] Ishikawa M, Murai Y, Wada A, Iguchi M, Okamoto K, Yamamoto F (2000) A novel algorithm for particle tracking velocimetry using the velocity gradient tensor. Exp. In Fluids 29
[9] Kitzhofer J, Brücker C, Pust O (2009) Tomo PTV using 3D Scanning Illumination and telecentric Imaging. Proceedings of the 8th International Symposium on Particle Image Velocimetry, Melbourne, Australia
[10] Maas HG, Westfeld P, Putze T., Botkjaer N, Kitzhofer J, Brücker C (2009) Photogrammetric techniques in multi-camera tomographic PIV. Proceedings of the 8th International Symposium on Particle Image Velocimetry, Melbourne, Australia